

BEHAVIOR OF DENSE GAS CLOUDS RELEASED SUDDENLY INTO A  
TURBULENT BOUNDARY LAYER

by

R. N. Meroney<sup>1</sup>

and

A. Lohmeyer<sup>2</sup>

Fluid Mechanics and Wind Engineering Program  
Civil Engineering Department  
Colorado State University  
Fort Collins, CO 80523

prepared for

6th International Conference on Wind Engineering - 1983  
Gold Coast, Queensland, Australia  
21-25 March 1983

1. Colorado State University, Fort Collins, Colorado.
2. University of Karlsruhe, Karlsruhe, FRG

August, 1982

CEP82-83RNM-AL2

# BEHAVIOR OF DENSE GAS CLOUDS RELEASED SUDDENLY INTO A TURBULENT BOUNDARY LAYER

R.N. Meroney<sup>1</sup> and A. Lohmeyer<sup>2</sup>

<sup>1</sup>Civil Engineering Department, Colorado State University, Fort Collins, CO 80523 (USA)

<sup>2</sup>Institute Wasserbau III, Univ. Karlsruhe, Karlsruhe 1, FRG

## ABSTRACT

The behavior of dense gas volumes emitted instantaneously into a simulated atmospheric boundary layer are compared to a numerical volume-integrated box model. Three different size source volumes were released into five different wind fields. The dense clouds were rapidly diluted to low values of concentration by gravity induced entrainment velocities.

## 1. INTRODUCTION

Sudden release of a dense gas near the ground is accompanied by horizontal spreading caused by gravitational forces. Such clouds will drift downwind from the source location at ground level, providing an opportunity for ignition if the gas is flammable or perhaps for acute toxic effect to life in its path. When the buoyancy forces are large they tend to dominate cloud shape, inhibit advection by the wind, and suppress dispersion by atmospheric turbulence.

Restricting attention to instantaneous volume source behavior one finds field experiments performed on the sudden release of Freon-12 with an initial mixed specific gravity of 1.25, and spills of liquid natural gas (LNG) on land or water with initial specific gravities near 1.5 [ref.1,2,3,10]. Most recently, Picknett (1978) describes the release of air/Freon gas mixtures with initial specific gravities ranging from 1.03 to 4.17 [ref.4]. The LNG experiments are complicated by release mechanisms, and the recent Freon experiments may suffer from instrument placement problems [ref.5]. Equivalent laboratory experience is limited to various lock-exchange experiments in water where the initial depth ratio of current to intruded fluid is often significant or to finite time releases of heavy gases from area sources [refs.6,7,8,9,10].

In a set of experiments preliminary to those discussed herein, Lohmeyer, Meroney, and Plate (1981) released small volumes of Freon-12 in a wind tunnel by permitting a known bubble volume of gas to rise through a liquid column and burst at the wind-tunnel ground surface (ref.11). Most of these experiments were performed in a calm environment.



This paper considers the results of wind-tunnel experiments performed to examine the behavior of dense plumes during periods of gravity spread/air entrainment dominance. A modified box model is presented to provide a framework of interpretation for the experiments. The experimental equipment and procedures are described. Finally, the data are evaluated and the order of magnitude of entrainment constants specified.

## 2. BOX MODEL FOR DENSE GAS CLOUDS

Consider a dense cloud which is instantaneously released as a cylindrical box of radius,  $R_i$ , and height,  $H_i$ , that undergoes a slumping motion in which  $R$  increases with time. As the motion proceeds one may assume the box mixes with ambient air, but maintains uniform properties internally. The radial velocity is assumed to vary linearly from zero at the center to a maximum at the outer edge of the cloud. Entrainment may occur over the upper cloud surface and at the front edge. Model details are contained in Appendix A of Meroney and Lohmeyer [ref.12].

Frontal spread velocities are calculated from a modified version of the total energy budget equation suggested by van Ulden [ref.13]. Dilution of the gas cloud occurs by entrainment across the upper cloud surface and the frontal area. These entrainment rates are adjusted to account for stratification modified gravity spread rate and background turbulence. Finally, although some models propose to relate drift distance to drift time by a normal wind speed (i.e.,  $x \cong u_R t$ , where  $u_R$  is a reference velocity), the current calculations use a cloud arrival time related to a logarithmic wind profile.

The final equations developed were nondimensionlized with respect to time and space scales equal to  $T = V_i^{1/6} (g'_i)^{-1/2}$  and  $L = V_i^{1/3}$  respectively where  $g'_i = g(SG_i - 1)$ . Nondimensional variables are indicated by a superscript star (\*). The final expressions used are

### Energy Equation:

$$\frac{du^*}{dt^*} = \frac{2}{\pi} \frac{1}{R^{*3}} - \frac{c_r u^{*2}}{R^*} - \frac{c_z u^{*2}}{2 H^*} \left[ 1 + \frac{\Delta p_i / \rho_a}{\psi^*} \right]^{-1} - 2 \beta_1 \frac{u^{*2}}{R^*} \quad (1)$$

$$\text{for } t^* < Ri_*^{1/2}$$

### Radial Growth Equation:

$$\frac{dR^*}{dt^*} = u_g^* \quad , \quad \text{but never less than} \quad (2a)$$

$$\frac{dR^*}{dt^*} = \frac{\alpha_7}{Ri_*^{1/2}} \quad (2b)$$

### Dilution Equation:

$$\frac{dV^*}{dt^*} = \pi R^{*2} u_z^* + 2\pi R^* H^* u_r^* \quad (3)$$

### Advection Equation:

$$\frac{dx^*}{dt^*} = u_g^* + \frac{1}{Ri_*^{1/2} k} \ln(\beta_2 \frac{H^*}{z_o^*}) \quad (4)$$

### Entrainment Relations:

$$\text{where } u_r^* = c_r u_g^* \quad (5a)$$

$$u_z^* = c_z u_g^* + \frac{\alpha_4 Ri_*^{-1/2}}{\frac{\alpha_4}{\alpha_6} + \frac{Ri_*}{\pi R^{*2}} \left[ 1 + \frac{\Delta\rho_i/\rho_a}{V^*} \right]^{-1}} \quad (5b)$$

$$Ri_* = (g_i') v_i^{1/3} / u_*^2 \quad (6)$$

$$\text{and } \chi = (V^*)^{-1} \quad \text{and } R^{*2} H^* \chi = 1. \quad (7)$$

Constants found to fit the various data most satisfactorily are  $c_r = c_z = 0.1$ ,  $\beta_1 = 0.9$ ,  $\alpha_4 = 2.6$ ,  $\alpha_6 = 0.39$ ,  $k = 0.4$ ,  $\beta_2 = 0.1$ , and  $\alpha_7 = 3.5$ . The Boussinesq assumption was not made during the development of these expressions. Equations (1), (2), (3) and (4) were integrated by a fourth-order Runge-Kutta scheme. Note that the cloud dispersion is only a function of initial cloud geometry (i.e.,  $R_i/H_i$  ratio), Richardson number,  $Ri_*$ , and surface roughness length,  $z_o^*$ , and initial specific gravity.

## 3. EXPERIMENTAL CONFIGURATION

An experiment was designed to examine the dispersion of instantaneous volumes of dense gas released at groundlevel in a wind tunnel capable of simulating the atmospheric boundary layer. The gases were released as initially half cylindrical clouds and the concentrations were monitored by an aspirated-hot-wire katherometer.

### 3.1 Wind Tunnel and Source Generation Equipment

The open circuit wind tunnel used had a test section 0.5 m high, 1.5 m wide, and 5 m long. At the tunnel entrance was a dense honeycomb and a vortex spire/barrier flow conditioner arrangement which produced a 30 cm deep turbulent shear layer which reached equilibrium and remained stationary over the final 3 meters of the test section. A 14 cm x 16 cm x 12 cm deep container of



water was maintained flush to the test section floor 2.5 meters from the entrance as noted in Figure 1. The rectangular box contained an apparatus to fill a half cylinder cup with dense gas, to raise the filled cylinder above the water surface until it stood exposed to the wind, but isolated by a water seal, and to suddenly rotate the horizontal cylinder about its axis, leaving a volume of dense gas almost motionless above the water surface. The cup rotated  $180^\circ$  in less than  $1/20$  second. A small magnet on the cup activated a reed switch which provided a voltage pulse to timing instrumentation.

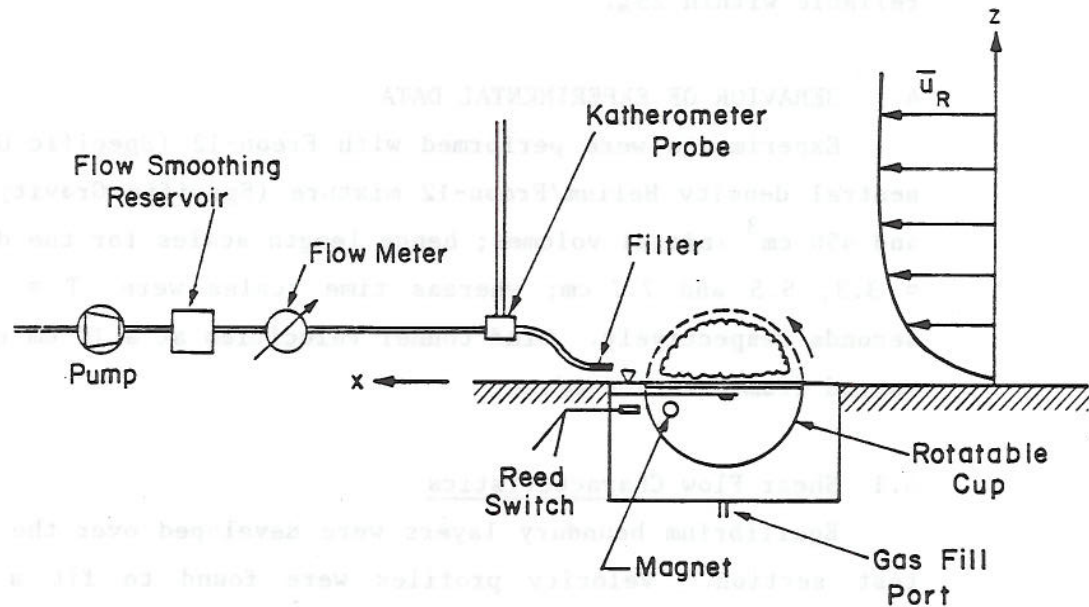


Fig. 1. Experimental configuration.

### 3.2 Concentration Measurements

Dense gas concentrations were measured with an aspirated hot film anemometer (katherometer) constructed from a DISA 55E07 mass flow transducer. The aspiration velocity at the 1 mm diameter probe tip was set at 0.1 m/sec to assure approximately isokinetic sampling of the plume. A fiber filter was present at the probe tip to reduce system sensitivity to pressure perturbations during shear flow measurements. All tests were corrected for a slight time lag required for the sample to travel through the probe to the detection wire. Extensive tests indicate such a probe has a flat frequency response to 150 Herz, concentration sensitivity to 0.10 percent, and resolution within  $\pm 5$  percent of a measurement [ref.14,15]. Since the probe is subject to drift and temperature effects it was recalibrated frequently. No significant deviations were detected.

During each realization of a volume release the katherometer response was registered on a chart recorder. Each sample point was recorded a minimum of five times. Time response was displayed within a resolution of  $t = \pm 0.1$  sec ( $t^* \leq \pm 3$ ).

### 3.3 Shear Flow Measurements

The extremely low speeds (0.0 to 0.4 m/sec) that were required to simulate the dense cloud drift necessitated the use of special calibration procedures for the hot wire anemometer used to measure velocities and turbulence. DISA 55A22 hot wires monitored by a DISA 55D01 anemometer were calibrated in a low speed nozzle whose speed was set with low-volume flow-rators. Velocity and turbulence measurements were made over the test section to detect the presence of any secondary cross currents. Velocities are reliable within 25%.

## 4. BEHAVIOR OF EXPERIMENTAL DATA

Experiments were performed with Freon-12 (Specific Gravity = 4.17) and a neutral density Helium/Freon-12 mixture (Specific Gravity  $\cong$  1.0) and 35, 165, and 450 cm<sup>3</sup> initial volumes; hence length scales for the dense releases were  $L = 3.3, 5.5$  and  $7.7$  cm; whereas time scales were  $T = .032, .042,$  and  $.049$  seconds respectively. Wind tunnel velocities at a 10 cm reference height were varied from 0 to 1.0 m/sec.

### 4.1 Shear Flow Characteristics

Equilibrium boundary layers were developed over the last 3 meters of the test section. Velocity profiles were found to fit a power law exponent  $p = 0.13$  above 1 cm and to fit a logarithmic velocity profile over most of the boundary layer with  $u_*/u_R \cong 0.048$  and  $z_o = 2.4 \times 10^{-5}$  m. Characteristic Richardson numbers,  $Ri_* = g_i' v_i^{1/3} / u_*^2$ , varied from 445 to 26,000 and  $\infty$  at calm conditions. Local longitudinal turbulence intensities were about 20% at the predominant cloud layer height of 0.5 cm. Shear stresses were nearly constant over dispersion depths, vertical turbulence intensities were small,  $\sim 6\%$ . Evaluation of profile shape, turbulence intensities, and integral scales suggested the simulated boundary layer scale was between 1:1000 to 1:2000.

### 4.2 Dense Cloud Dispersion During Calms

Over the ten fold range of source volumes studied all radial growth and concentration decay behavior collapsed together when plotted as  $R^*$  vs  $t_a^*$ ,  $\chi_m$  vs  $t_a^*$ , and  $\chi_m$  vs  $R^*$ . The data also duplicated the earlier behavior of independent experiments performed by Lohmeyer et al. (1981) for 50 cm<sup>3</sup> source volumes released in a different wind tunnel using different instrumentation and release mechanism [ref.11]. Average data behavior are included with wind shear results discussed in the following paragraphs.



#### 4.3 Dense Cloud Dispersion with Wind Shear

The presence of a wind field influences the dispersing dense gas in the following manner. In a weak or moderate wind the cloud slumps rapidly. It spreads radially, but the portion moving upwind slows somewhat and thickens. Subsequently, the entire cloud begins to drift downwind. When gravity driven velocities fall below local wind field speeds, at  $t^*$  near  $Ri_* C_f/2$ , background turbulence and wind shear begin to enhance entrainment, and when gravity driven velocities fall below  $u_*$  at  $t^* \cong Ri_*$ , the shear flow completely dominates mixing.

Results from the experiments for varying wind shear are presented in Figures 2, 3, and 4. The downwind transport of a dense cloud in terms of dimensionless coordinates  $x^*$  and  $t_a^*$  is shown in Figure 2. One notes the regular decrease in cloud arrival time as  $u_R^*$  increases (as  $Ri_*$  decreases). The clouds appear to accelerate toward background advection speeds only after an initial inertial hesitation. The cloud appears to remain stationary for  $t_a^* < 10$ .

Figures 3 and 4 describe plume dilution  $\chi_m$  versus  $t_a^*$  and  $x^*$  respectively. Plume concentrations decay asymptotically as  $(t_a^*)^{-3/2}$  and  $(x^*)^{-3}$  during calm situations. For wind shear situations concentration variation with arrival time behaves in a rather irregular manner depending on initial cloud size. For the smallest cup size increasing wind speed results in progressively faster concentration decay rates. For the medium and large cup sizes initially small wind velocities result in apparently lower concentration decay rates, as the clouds are convected downwind without a proportionally higher rate of dilution. At higher wind speeds the cloud dilutes faster, the decay rate increases, and the slope of the  $\chi_m$  vs  $t_a^*$  curves steepen again.

As shown in Figure 4 concentrations universally increase downwind with wind speed compared to the calm situation; however, the data suggests for each cloud size and downwind location a wind speed exists which results in maximum concentrations measured. At higher wind speeds one expects the added diluting capacity of the atmosphere to cause concentrations to vary inversely with wind speed for a fixed source rate.

Figure 5 emphasizes again the influence of wind shear by examining the variation of  $t_a^*$  and  $\chi_m$  when  $x^*$  is held constant and the variation of  $\chi_m$  when  $t_a^*$  is held constant. No strong source size perturbation is apparent in the distribution of arrival times; however, source size obviously influences concentrations at low wind speeds. As  $u_R^*$  becomes large  $\chi_m$  appears to approach similar values for all source sizes studied at the given  $t_a^*$ .

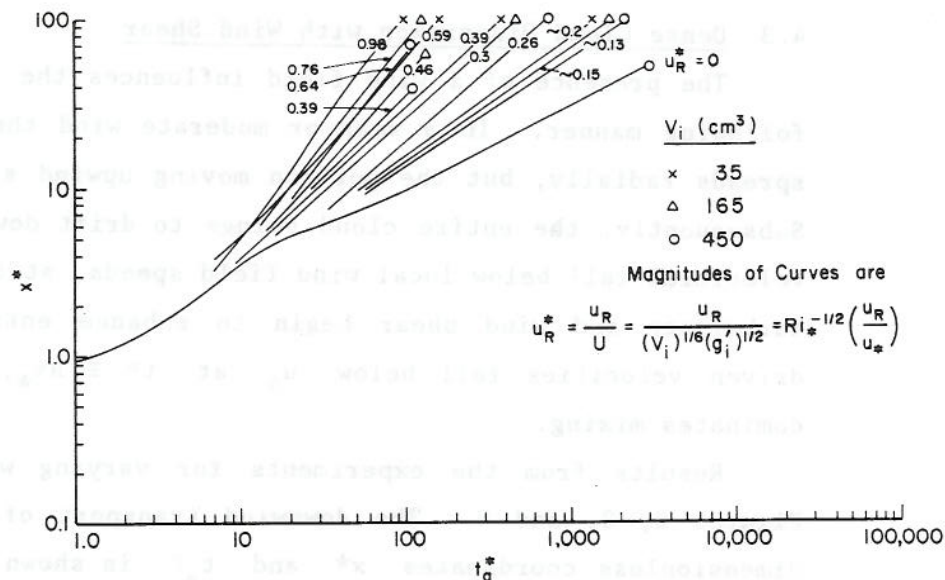


Fig. 2. Cloud transport distance versus arrival time.

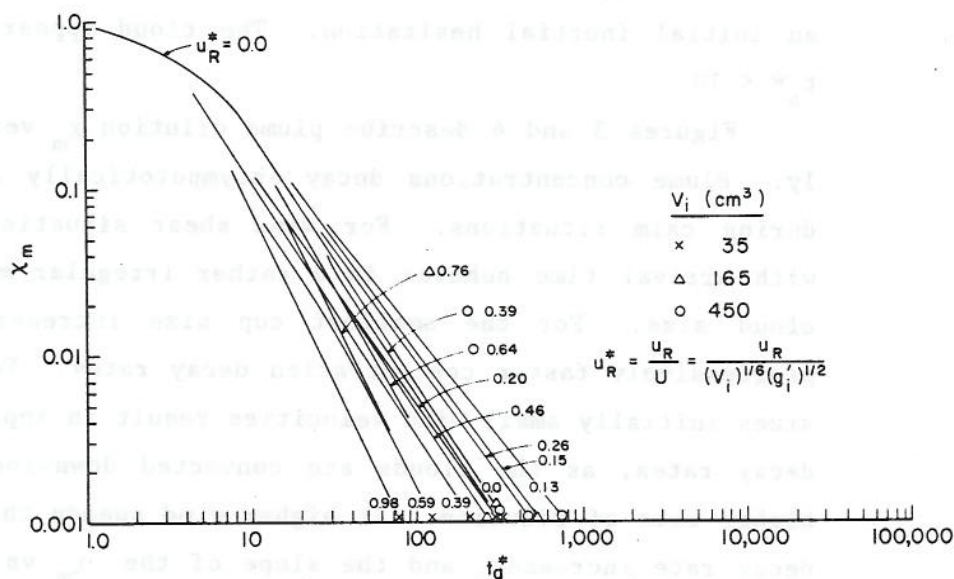


Fig. 3. Cloud dilution versus arrival time.

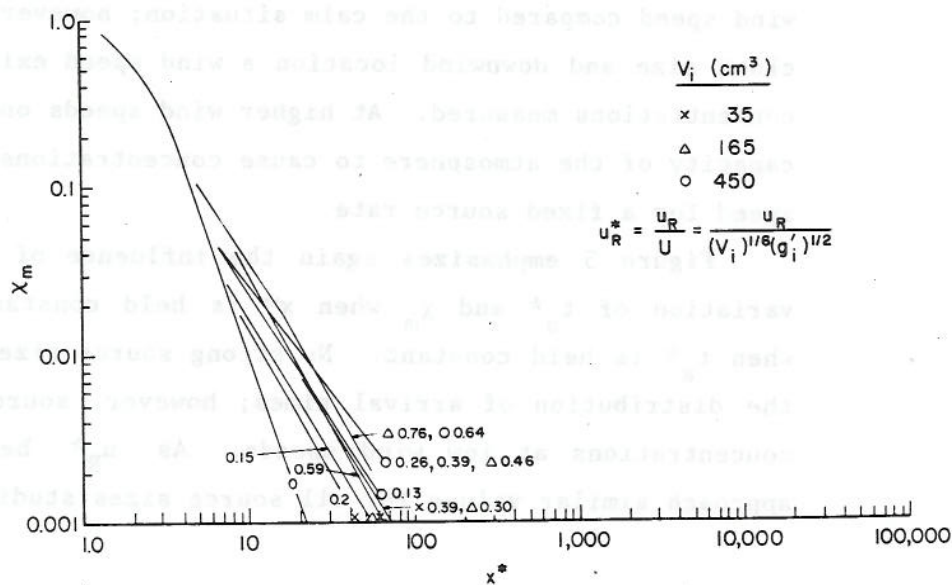


Fig. 4. Cloud dilution versus downwind distance.



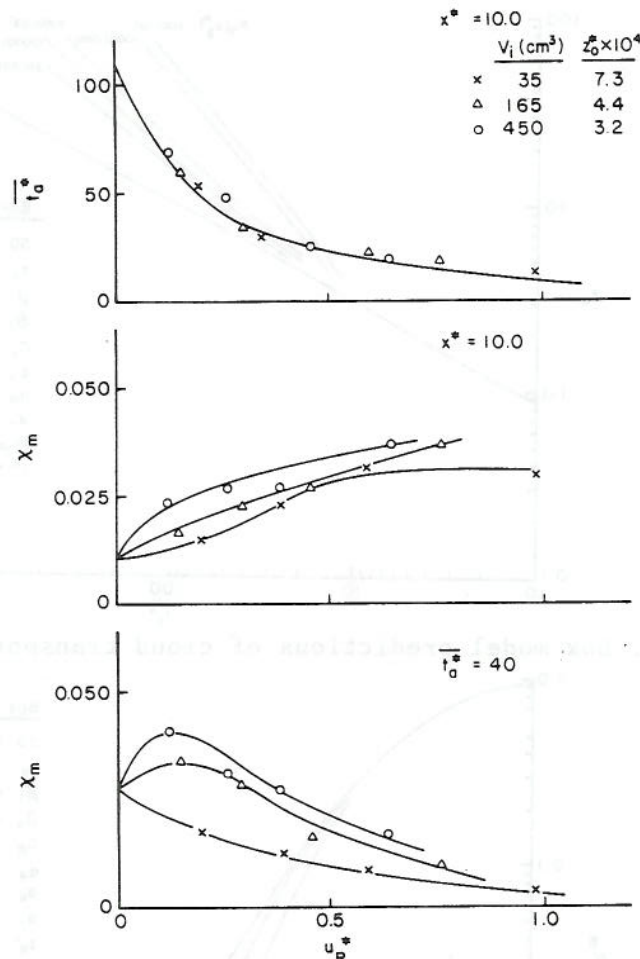


Fig. 5. Variation of arrival time and concentration with velocity.

## 5. BEHAVIOR OF NUMERICAL BOX MODEL

The volume-averaged box model discussed earlier can reproduce radial cloud dimensions and maximum concentrations measured during calm conditions within experimental error and statistical scatter. It can not reproduce the actual vertical and radial variations of height, concentration and velocity in time. Indeed, if the box model is designed to reproduce maximum concentrations measured at various radial locations, then the bulk average concentrations predicted will always be too low, and the entrainment rates too high for the reality of local entrainment physics. Nonetheless, such a model has engineering value and it is important to evaluate its limitations.

### 5.1 Comparison to Wind-Tunnel Experiments

Cloud transport distance calculated is plotted versus arrival time in Figure 6. The behavior is quite similar to that measured in Figure 2. Cloud dilution is plotted versus arrival time in Figure 7 and distance in Figure 8. Here the limitations of the box model become apparent. Due to the well mixed cloud assumption the model can not reproduce the lower decay rates at low wind speeds and higher decay rates at high wind speeds. The box model does reproduce the set of curves representative of higher mixing rates at the higher

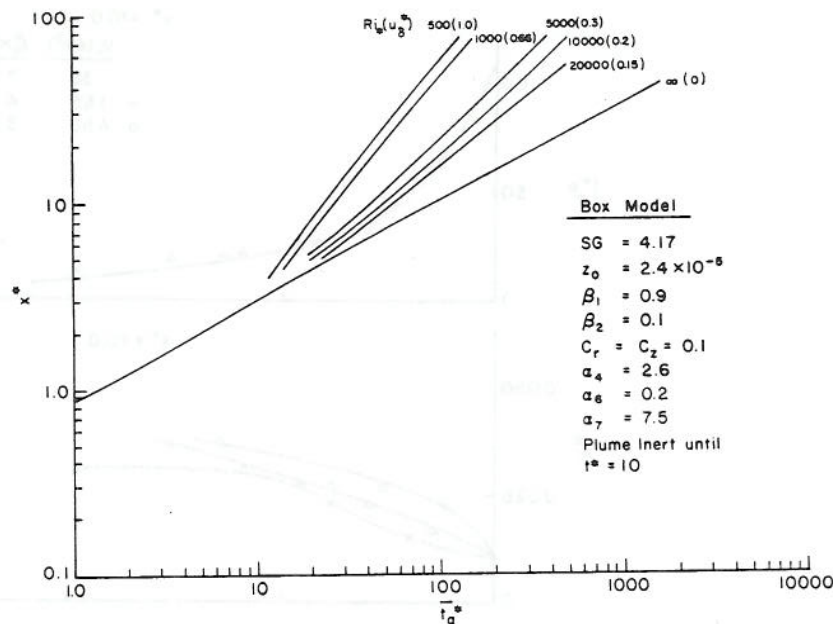


Fig. 6. Box model predictions of cloud transport distance.

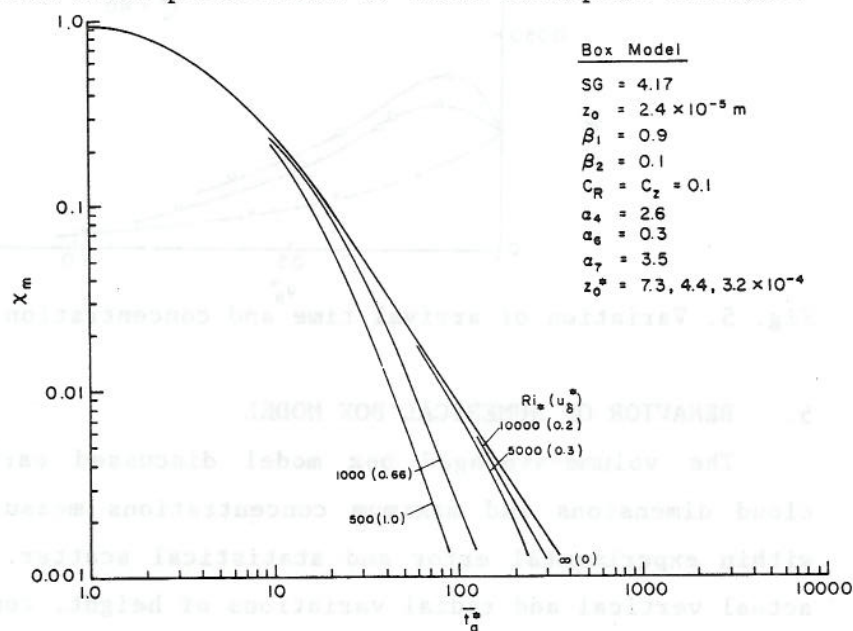


Fig. 7. Box model prediction of cloud dilution versus arrival time.

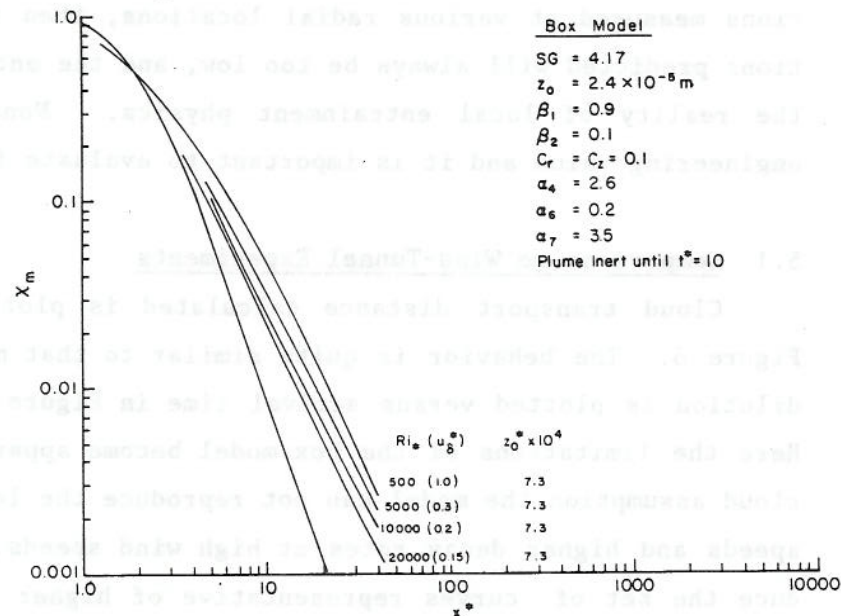


Fig. 8. Box model prediction of cloud dilution versus downwind distance.



Box Model SG = 4.7,  $z = 2.4 \times 10^{-3}$   
 $\beta_1 = 0.9$ ,  $C_r = 0.1$ ,  $a_4 = 2.5$ ,  $a_7 = 3.5$   
 $\beta_2 = 0.1$ ,  $C_z = 0.1$ ,  $a_6 = 0.3$ ,  
 Plume inert until  $t^* = 1.0$

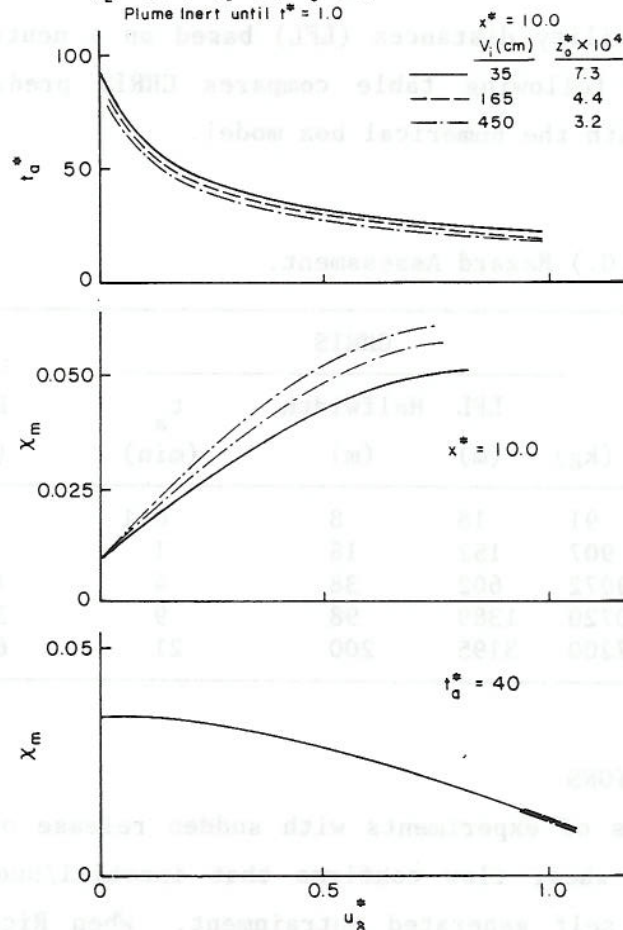


Fig. 9. Variation of arrival time and concentration with velocity, box model predictions.

velocities. It also predicts higher concentrations at a given distance with higher wind speeds. The limiting decay rates at low concentrations behave as  $\chi_m \sim t_a^{*-1/3}$  and  $\chi_m \sim x^{*-1/3}$  at large times.

To illuminate the independent effects of  $Ri_*$  and  $z_o^*$  the box model results were plotted as shown in Figure 9. Comparable data is found on Figure 5. The box model results are generally similar, but they do not reproduce the sources of roughness effect found in the plots of dilution versus wind speed. Nonetheless, for such a simple model the predictions are respectable.

## 5.2 Prediction of Propane Cloud Behavior

The box model was used to predict a range of hazard distances produced by instantaneous spills of propane or L.P.G. The results are limited to flat terrain, uninterrupted by surface obstacles, a neutrally stable atmosphere (Pasquill-D), roughness  $z_o \cong 2$  cm, and surface drag  $u_* / u_R \cong 0.05$ . The most widely used hazard assessment and response tool currently used by fire departments and other emergency response agencies in the USA is the Chemical Hazard Response Information System (CHRIS) [ref.16]. This methodology calculates

lower flammability distances (LFL) based on a neutral density Gaussian plume model. The following table compares CHRIS predictions for various spill situations with the numerical box model.

TABLE 1

Propane (L.P.G.) Hazard Assessment.

Spill Sizes (short tons) (kg)		CHRIS			BOX		
		LFL (m)	Halfwidth (m)	$t_a$ (min)	LFL (m)	Halfwidth (m)	$t_a$ (min)
0.1	91	18	8	0.1	30	28	0.50
1.0	907	152	18	1	66	60	1.00
10.0	9072	602	38	4	140	127	1.25
100.0	90720	1389	98	9	300	275	2.00
1000.0	907200	3195	200	21	650	600	2.67

## 6. CONCLUSIONS

A series of experiments with sudden release of dense gas volumes at the ground in a shear flow confirms that inertial/buoyant spreading is rapidly followed by self generated entrainment. When Richardson numbers are sufficiently large, the gas may be diluted well below flammable or toxic limits before the effects of shear turbulence are evident. No previous numerical dense cloud model has been evaluated with respect to such a large set of controlled and repeated experiments.

## ACKNOWLEDGMENTS

The authors wish to acknowledge support from the Institute Wasserbau III, University of Karlsruhe, and the von Humboldt Foundation, F.R.G. Report and paper preparation were supported by the Gas Research Institute, U.S.A., under contract No. 5014-352-0203.

## REFERENCES

1. A.P. van Ulden, On the Spreading of a Heavy Gas Released Near the Ground, Proceedings of First International Loss Prevention Symposium, the Hague/Delft, Elsevier, Amsterdam, 1974, pp. 431-439.
2. American Gas Association, LNG Safety, Program Interim Report on Phase II Work, AGA Project IS-3-1 Battelle, Columbus Laboratories, 1974.
3. G.F. Feldbauer, J. Heigl, W. May et al., Spills of LNG on Water-Vaporization and Downwind Drift of Combustible Mixture, Rpoert Nr. ZE6IE-72, Esso Research and Engineering Co., Florham, Park, New Jersey, 1972.
4. R.G. Picknett, Fluid Experiments on the Behavior of Dense Clouds, Part I, Main Report, Ptn 1 L 1154/78/1, Chemical Defence Establishment, Porton Down, U.K., 1978.
5. J.A. Fay, Gravitational Spread and Dilution of Heavy Vapor Clouds, Second International Symposium on Stratified Flows, Trondheim, Norway, 24-27 June 1980, pp. 421-494.



6. T. Maxworthy, On the Formation of Nonlinear Internal Waves from the Gravitational Collapse of Mixed Regimes in Two and Three Dimensions, J. Fluid Mech., 99, Part 1, 1980, pp. 47-64.
7. H.E. Huppert and J.E. Simpson, The Slumping of Gravity Currents, J. Fluid Mech., 99, 1980, pp. 785-799.
8. T.B. Benjamin, Gravity Currents and Related Phenomena, J. Fluid Mech. 31, 1968, pp. 209-248.
9. D.J. Hall, Further Experiments on a Model of an Escape of Heavy Gas, Report LR (312) AP, Warren Springs Laboratory, Stevenage, Herts, U.K., 1974.
10. R.N. Meroney and D.E. Neff, Physical Modeling of Forty Cubic Meter LNG Spills at China Lake, California, Air Pollution Modeling and Its Applications, C. de Wispelaere, (Ed.) Plenum Publishing Corp., 1980, pp. 24-27.
11. A. Lohmeyer, R.M. Meroney, and E. Plate, Model Investigations of the Spreading of Heavy Gases Released from an Instantaneous Volume Source at the Ground, Air Pollution Modeling and Its Applications, Vol. 1, C. de Wispelaere (Ed.), Plenum Publishing Corp., 1981, pp. 433-448.
12. R.N. Meroney and A. Lohmeyer, Gravity Spreading and Dispersion of Dense Gas Clouds Released Suddenly into a Turbulent Boundary Layer, Colorado State University Research Report CER82-83RNM-AL-7, Fort Collins, Colorado, 1982.
13. A.P. van Ulden, The Unsteady Gravity Spread of a Dense Cloud in a Calm Environment, 10th International Technical Meeting on Air Pollution Modeling and Its Application, NATO-CCMS, Rome, Oct. 26, 1979, 9 pp.
14. R.N. Meroney, D.E. Neff, and J.E. Cermak, Wind-Tunnel Modeling of LNG Spills, American Gas Association Transmission Conference, 8-10 May, Montreal, Canada, 1978, 26 pp.
15. D.J. Wilson and D.D.J. Netterville, A Fast Response Heated Element Concentration Detector for Wind Tunnel Applications, to appear in Journ. Industrial Aerodynamics, 1980, 21 pp.
16. M.C. Parnarouskis, M.F. Flessner, and R.G. Potts, A Systems Approach to Chemical Spill Response Information Needs, Hazardous Chemicals - Spills and Waterborne Transportation, S. S. Weidenbaum (Ed.), Amer. Inst. of Chem. Engineers Symposium Series, Vol. 76, No. 194, pp. 32-41.

NOTATION:

<u>Symbols</u>	<u>Definition</u>
$c_r, c_z$	Entrainment coefficients
$C_f/2$	Skin friction coefficient
$g^*$	Modified gravitational constant
$H$	Height of cloud
$k$	von Karman coefficient
$L$	Length scale
$p$	Power law coefficient
$R$	Cloud radius
$Ri_*$	Richardson number, Eq. (6)
$t$	Time
$t_a$	Cloud arrival time at $x$
$T^a$	Time scale
$u$	Friction velocity
$V^g$	Cloud volume
$x$	Downwind distance
$z$	Roughness length
$\alpha_i, \beta_i$	Various constants in Eqs. (1) to (5)
$\chi$	Plume dilution, volume or mole fraction
<u>Subscripts</u>	
$i$	Initial cloud property
$a$	Property at ambient air
$R$	Evaluated at reference height ( $z_R = 10$ cm)
<u>Superscript</u>	
$*$	Nondimensional quantity

